nature nanotechnology

ARTICLES

PUBLISHED ONLINE: 7 OCTOBER 2012 | DOI: 10.1038/NNANO.2012.170

In situ atomic-scale imaging of electrochemical lithiation in silicon

Xiao Hua Liu[1]*, Jiang Wei Wang[2], Shan Huang[3], Feifei Fan[3], Xu Huang[4], Yang Liu[1], Sergiy Krylyuk[5,6], Jinkyoung Yoo[7], Shadi A. Dayeh[7], Albert V. Davydov[5], Scott X. Mao[2,8], S. Tom Picraux[7], Sulin Zhang[4], Ju Li[9], Ting Zhu[3]* and Jian Yu Huang[1]*

In lithium-ion batteries, the electrochemical reaction between the electrodes and lithium is a critical process that controls the capacity, cyclability and reliability of the battery. Despite intensive study, the atomistic mechanism of the electrochemical reactions occurring in these solid-state electrodes remains unclear. Here, we show that *in situ* transmission electron microscopy can be used to study the dynamic lithiation process of single-crystal silicon with atomic resolution. We observe a sharp interface (~1 nm thick) between the crystalline silicon and an amorphous Li_xSi alloy. The lithiation kinetics are controlled by the migration of the interface, which occurs through a ledge mechanism involving the lateral movement of ledges on the close-packed {111} atomic planes. Such ledge flow processes produce the amorphous Li_xSi alloy through layer-by-layer peeling of the {111} atomic facets, resulting in the orientation-dependent mobility of the interfaces.

Lithium-ion batteries are increasingly being used as energy storage devices in portable electronics and transportation vehicles[1]. The electrochemical reaction in the electrodes is a subject of great interest[2–7] in the quest to develop high-performance electrode materials that can radically improve the capacity, rate and cyclability of these batteries. In this regard, nanomaterials such as nanoparticles and nanowires are being extensively studied as the building blocks of next-generation electrodes[8–10]. This is motivated by the notion that their nanometre dimensions can shorten the electron and ion transport paths and enable facile strain relaxation, thus enhancing both the rate capability and flaw tolerance of the nanomaterial-based electrodes[4,8]. Nanomaterials are generally produced in the crystalline form. The first lithiation of these nanomaterials at room temperature thus involves solid-state amorphization, particularly in silicon, a promising anode material with an extremely high theoretical capacity (3,579 mAh g^{-1} at room temperature) for lithium-ion batteries[11,12]. It is also being increasingly recognized that the solid-state amorphization during silicon lithiation could have a significant impact on stress generation and fracture, leading to capacity fading[2]. Although recent studies of lithiated silicon have revealed the formation of sharp interfaces between crystalline silicon (c-Si) and amorphous Li_xSi (a-Li_xSi) alloy[13–15], there is currently a lack of critical knowledge about the dynamic lithiation mechanisms. Revealing the atomic-level and real-time processes of lithiation is crucially important for understanding the physical basis of microstructural evolution, morphological changes and mechanical degradation in silicon-based electrodes. The insights gained could therefore help in developing strategies to mitigate mechanical failure during electrochemical reactions.

Recently, the lithiation kinetics in a single-crystal silicon matrix were found to be highly anisotropic[13,16,17]. In other words, the rate of crystalline-to-amorphous phase transformation seems to depend strongly on the 'invasion direction' of the lithium, with ⟨111⟩ reported to be the slowest (meaning the {111} surfaces of the silicon exposed to Li^+-containing electrolyte would expand the slowest) and ⟨110⟩ appearing to be the fastest[17]. Generally speaking, the kinetics of phase transformation can be either (i) long-range transport controlled, (ii) short-range reaction and interfacial mobility controlled, or (iii) under mixed control[18]. In (i), most of the total free energy drop is spent on long-range diffusion of Li^+ ions and electron transport across the product/reactant phases, and little is spent locally near the phase interfaces, where the phase transformation occurs. In (ii), the opposite is true. As such, when considering the origin of the observed anisotropic lithiation, it is natural to ask whether the apparent anisotropy is caused mainly by (i) long-range transport or (ii) short-range reaction/interfacial mobility. If the latter is true, what is the atomistic origin of the anisotropic interfacial mobility?

Here, we report the atomistic mechanism of dynamic lithiation in single-crystal silicon, obtained by directly observing the electrochemical reaction of a nanoscale battery using an individual silicon nanowire inside a transmission electron microscope (TEM)[12,19]. We present atomically resolved dynamical images that clearly reveal a ledge mechanism of interfacial motion and solid-state amorphization.

Ledge mechanism of lithiation in c-Si

Figure 1 and Supplementary Movies S1,S2 show the lithiation of a silicon nanowire with a ⟨111⟩ growth direction. The pristine

[1]Center for Integrated Nanotechnologies, Sandia National Laboratories, Albuquerque, New Mexico 87185, USA, [2]Department of Mechanical Engineering and Materials Science, University of Pittsburgh, Pittsburgh, Pennsylvania 15261, USA, [3]Woodruff School of Mechanical Engineering, Georgia Institute of Technology, Atlanta, Georgia 30332, USA, [4]Department of Engineering Science and Mechanics, Pennsylvania State University, University Park, Pennsylvania 16802, USA, [5]Material Measurement Laboratory, National Institute of Standards and Technology, Gaithersburg, Maryland 20899, USA, [6]Institute for Research in Electronics and Applied Physics, University of Maryland, College Park, Maryland 20742, USA, [7]Center for Integrated Nanotechnologies, Los Alamos National Laboratory, Los Alamos, New Mexico 87545, USA, [8]Center for Electron Microscopy, Department of Materials Science and Engineering, Zhejiang University, Hangzhou 310027, China, [9]Department of Nuclear Science and Engineering and Department of Materials Science and Engineering, Massachusetts Institute of Technology, Cambridge, Massachusetts 02139, USA. *e-mail: lxhua99@gmail.com; ting.zhu@me.gatech.edu; jyhuang8@yahoo.com

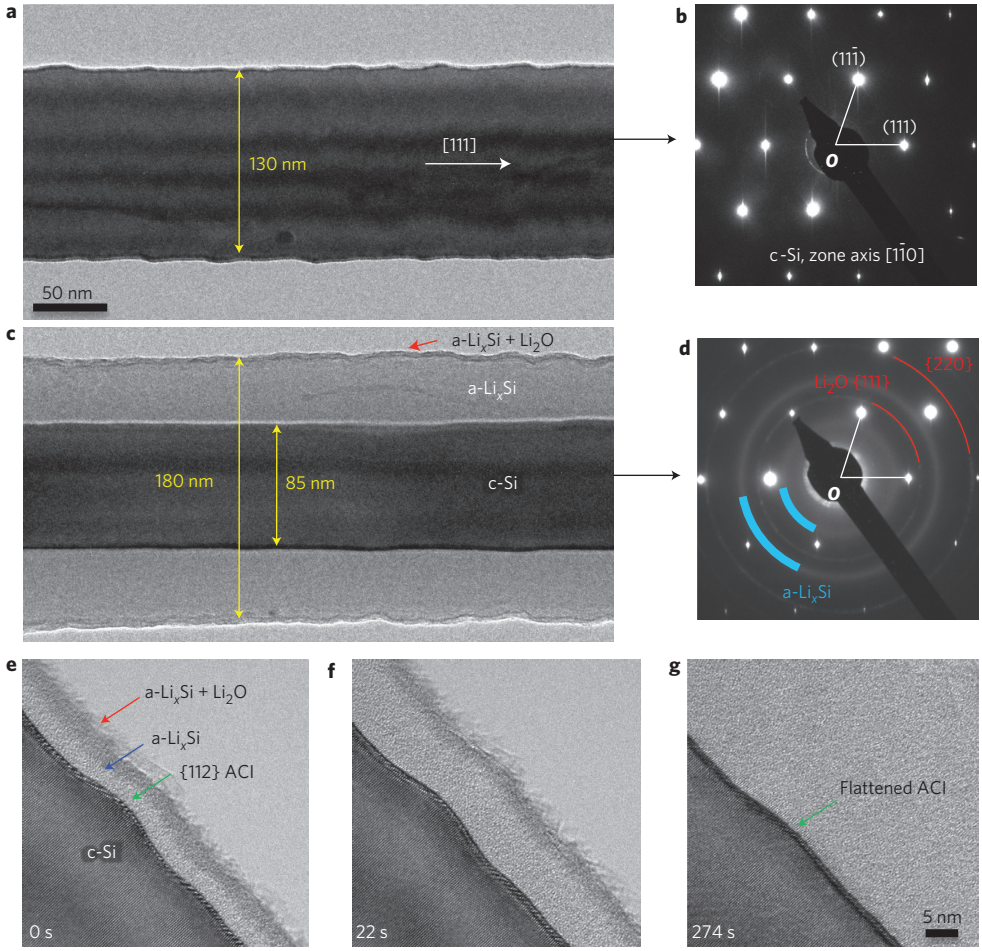

Figure 1 | Progressive migration of the sharp ACI during solid-state amorphization (lithiation) of a crystalline ⟨111⟩-oriented silicon nanowire. a, Pristine silicon nanowire with rough sidewalls due to faceting. **b**, Electron diffraction pattern from the pristine single-crystal silicon nanowire. **c**, Partially lithiated silicon nanowire with an a-Li$_x$Si layer surrounding the c-Si core. The ACI is sharp and flat. **d**, Corresponding electron diffraction pattern indicating the amorphization process. **e**–**g**, Time-lapse images showing migration of the {112} ACI during lithiation. The ACI is ~1 nm thick and did not change in thickness, but became smoother during progressive migration.

silicon nanowire is single crystalline with six faceted {112} side faces (Fig. 1a,b, Supplementary Fig. S1). Upon lithiation, a Li$_x$Si alloy shell is developed, which is amorphous with a grey contrast (Fig. 1c,d). The amorphous/crystalline interface (denoted ACI) is only ~1 nm thick and features a unique striped contrast (Fig. 1e–g). The outermost layer of the lithiated wire exhibits a darker contrast than the inner a-Li$_x$Si layer (Fig. 1c,e), and consists of a-Li$_x$Si and Li$_2$O, both of which result from the lithiation of the native SiO$_x$ that covered the sidewall of the silicon nanowire (Supplementary Fig. S1). The nanowire was viewed along the [1$\bar{1}$0] direction, and the ACI was mainly parallel to the (1$\bar{1}$2) plane. As the ACI migrated towards the wire centre, the c-Si core shrunk progressively. Meanwhile, the a-Li$_x$Si shell thickened dramatically due to the large radial expansion (yielding ~280% volume increase). Interestingly, the ACI did not change in thickness throughout the entire process (Fig. 1e–g). However, it became flatter, as demonstrated by the reduced height of the bump with respect to the baseline in Fig. 1g. It is known that ⟨111⟩-oriented silicon nanowires grown by the chemical vapour deposition method are usually saw-tooth-faceted on their sidewalls due to the lack of low-index planes parallel to ⟨111⟩ (Fig. 1a, Supplementary Fig. S1c)[20]. Initially, the ACI was nearly parallel to the sidewall, and therefore replicated the faceted surface morphology. As lithiation proceeded, the facets on the ACI diminished (Fig. 1c) as a result of the orientation-dependent interfacial mobilities of the ACI (discussed further later).

Figure 2 and Supplementary Movie S3 present close-up views of the atomic structures of an ACI and unambiguously reveal a ledge mechanism of c-Si lithiation. The seven arrows mark the ledges consisting of successive inclined (1$\bar{1}$1) atomic planes (Fig. 2a–c), and the red dot arrays represent a two-dimensional projection along the [1$\bar{1}$0] direction of the pristine silicon lattice in the silicon nanowire core (Fig. 2d). The high-resolution TEM images of Fig. 2a–c show that the atomic arrangement in the ACI is highly distorted and exhibits a unique striped contrast, which is clearly different from the perfect c-Si lattice in the inner core of nanowire. It also differs distinctly from the amorphous shell, which has a disordered structure, as the periodic feature in the ACI (that is, a short array of bright spots) is clearly resolvable. Dynamic observation of migration of the ACIs suggests a ledge-mediated mechanism of solid-state amorphization, with lithium atoms squeezed into the large open space between two neighbouring (1$\bar{1}$1) bilayers (that is, two closely spaced (1$\bar{1}$1) atomic planes, such as *Aa* in the diamond structure with *AaBbCc* stacking). This increases the (1$\bar{1}$1) bilayer spacing, leading to peeling of the top (1$\bar{1}$1) bilayer. Meanwhile, the ledges (that is, atomic steps) flow along the (1$\bar{1}$1) plane, and silicon atoms at the ledges are 'dissolved' into the a-Li$_x$Si phase. As a result, the lithiation reaction takes place by atomic removal

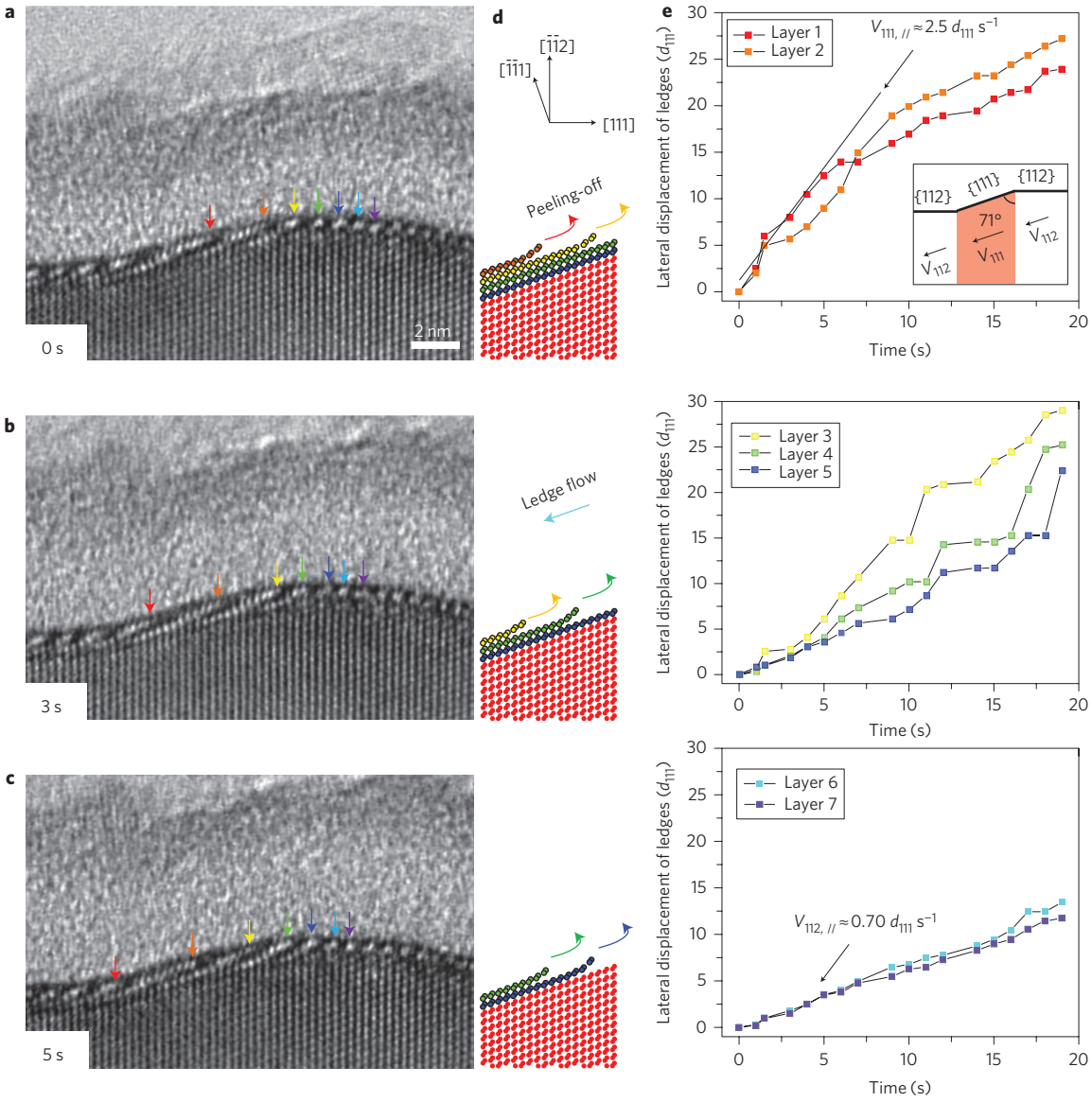

Figure 2 | Ledge mechanism of lithiation in c-Si. a–c, High-resolution TEM image sequences showing the lithiation process by lateral ledge flow (marked by coloured arrows) in the ACI and simultaneous peeling-off of the {111} planes over 5 s. The ACI is ~3–4 atomic layers thick, and the atomic layers are distorted and different from both the regular lattice in the bottom c-Si and the mottled contrast in the top a-Li_xSi layer. **d**, Schematic showing the peeling-off of the ($\bar{1}\bar{1}1$) atomic layers by continuous ledge flow in the planes during lithiation. **e**, Lateral displacement of the seven ledges projected to the horizontal [111] direction versus time. Ledges moved faster on the {111} facet and slower on the {112} planes. Ledge flow speed is inversely proportional to ledge density, giving a constant radial etching rate.

from the silicon surface (alloyed into the a-Li_xSi shell) during migration of ledges. Evidently, the peeling of the {111} facets occurs in a layer-by-layer manner and through lateral ledge flow in each layer, as illustrated in Fig. 2d. Figure 2e shows the lateral displacement (projected to the horizontal [111] direction) of the seven ledges versus time. Interestingly, in this short length scale of ~10 nm, with similar radial lithium flux from the nanowire surface to the centre, the speed of ledge flow is inversely proportional to the ledge density on the ACI, giving a nearly constant radial lithiation speed. When the ledges are on the inclined ($\bar{1}\bar{1}1$) facet they pass about 2.5 vertical (111) planes per second (spacing $d_{111} = 0.31$ nm), which is 3.5 times faster than the speed of $0.70 d_{111}\ s^{-1}$ observed when the ledges were sitting on the horizontal ($\bar{1}\bar{1}2$) ACI.

Although the atomically flat ($\bar{1}\bar{1}1$) facet shown in Fig. 2 is merely the local fine feature of the microscopic ($\bar{1}\bar{1}2$) ACI shown in Fig. 1e–g, it clearly indicates that lithium invasion into crystalline silicon occurs exclusively along the lateral ⟨110⟩ and ⟨112⟩ directions of the close-packed {111} planes by the ledge mechanism. Lithium penetration through {111} planes was never observed, although the {111} planes were directly exposed to the surrounding lithium sea, otherwise the lifting-off of a small {111} sheet should have also been observed in the *in situ* experiments. Atomic removal at the ledges of the c-Si {111} planes finally shortens the relatively long {111} facets in the ACIs, changing the low-ledge-density ACIs into ACIs with high ledge densities, such as {112} and {110}. We have also directly visualized the migration of the {110} ACIs by rotating the silicon nanowires about the [111] axis (Supplementary Movie S4), which compares the different morphologies of the ACIs that were dependent on the crystallographic orientations of the silicon. The TEM images in Supplementary Fig. S2 indicate that the {110} ACI is still narrow (~1 nm wide),

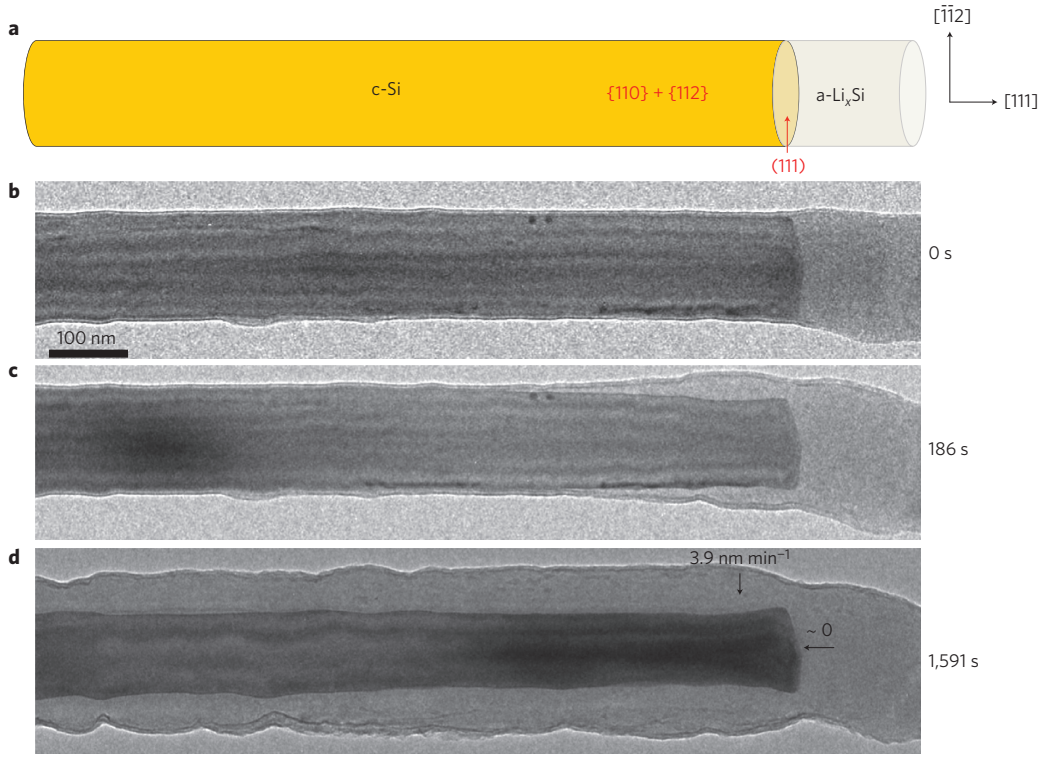

Figure 3 | Comparison of the migration speed of the different ACIs. a,**b**, Starting structure of a partially lithiated ⟨111⟩-oriented silicon nanowire. The nanowire has a flat (111) cross-section and is surrounded by {110} and {112} planes. This structure was created with a transient high potential (−50 V), which transforms the conventional core–shell lithiation mechanism to an axial lithiation mechanism. **c**, Under conventional lithiation conditions of a −2 V potential and weak electron beam, lithiation occurs along the radial directions but not along the axial direction. **d**, Core–shell structure after exclusive radial lithiation. The average migration speed was 3.9 nm min^{-1} for the {110} and {112} ACIs, but nearly zero for the {111} ACI.

but rough and blurred, in contrast to the clearly visible lattice structure of the {112} and {111} ACIs.

Orientation-dependent interface mobility

On a larger length scale, lithiation on a macroscopic {111} face (that is, a large {111} facet without significant ledges) is kinetically unfavourable due to the lack of active {111} ledges exposed to lithium as well as the difficulty of creating a ledge pair, that is, a lithiated island in the next {111} layer of c-Si. Figure 3 shows that at a length scale of 100 nm, the (111) cross-section is almost immobile, while substantial lithiation occurs on the adjacent {110} + {112} sidewalls. In such a ⟨111⟩-oriented silicon nanowire nominally enclosed by {110} and {112} planes, the migration velocity of the ACIs parallel to the sidewalls, $v_{\{110\}+\{112\}}$, was measured to be ~3–5 nm min^{-1}, but the motion of the {111} ACI, $v_{\{111\}}$, was not measurable under similar conditions (that is, electron beam irradiation and local chemical composition). This is consistent with previous studies that have shown significant swelling along the ⟨110⟩ direction but negligible swelling along the ⟨111⟩ direction if both {110} and {111} faces are exposed[13,17]. We observed similar migration velocities for both {110} and {112} ACIs. The comparable lithiation speeds along the radial ⟨110⟩ and ⟨112⟩ directions lead to nearly isotropic expansion of cross-sections of the ⟨111⟩-oriented silicon nanowires[16]. Compared with the dynamically diminishing {111} ACIs, the {112} and {110} ACIs were atomically rough but microscopically flat, and their migration was steady and lacking features such as flowing ledges.

The atomically resolved observations provide insight into the origin of why the {112} ACI moves faster than the {111} ACI. To clarify the terminology, from here on we will use '{111} atomic facet' to mean an individual short facet in a long ACI, and '{112} or {111} ACI' to mean a long interface that takes on average the {112} or {111} planes, but may consist of many short {111} atomic facets and ledges, thus having finite, atomic-scale roughness. Figure 4a presents a high-resolution TEM image of a {112} ACI at the initial stage of lithiation, in which a long ($\bar{1}\bar{1}$1) facet with a width of ~15 nm can be seen. Figure 4b shows a typical flattened {112} ACI after the large {111} atomic facets have been removed by the peeling process of lithiation. The inset of Fig. 4a shows a magnified TEM image near a {112} ACI, the atomic structure of which is reconstructed in Fig. 4c. As schematically shown in Fig. 4d, an exact {112} surface in c-Si is composed of a series of inclined {111} atomic facets. Each facet consists of four {111} bilayers (indicated by pink dashed lines), and is thus ~1 nm (or $3d_{111}$) wide. Geometrically, the translational periodicity within an exact {112} surface is governed by that of the diamond-cubic silicon lattice; for example, the periodicity in the horizontal ⟨111⟩ direction is simply the diagonal length of the ⟨001⟩ × ⟨011⟩ rectangular box in Fig. 4d. As a result, the {111} atomic facets in the inset of Fig. 4a (blue segments) are the smallest possible structural units for building an exact {112} surface. Because of the small width of the {111} atomic facets, there is a high density of ledges associated with the {112} ACI. Such ledges act as heterogeneous sites to facilitate the Si–Li reactions, giving rise to a high mobility of the {112} ACI. Similarly, the {110} ACIs geometrically consist of a high density of inclined {111} atomic facets, explaining the similar mobilities of the {110} and {112} ACIs. It is also interesting to see from Fig. 4a that one atomically flat {111} ACI lay initially between two atomically rough {112} ACIs. However, this {111} ACI was not stable, and only {112} ACIs remained in the late stage of lithiation, as shown in Fig. 4b.

The above atomically resolved observations also suggest an efficient kinetic mechanism of solid-state amorphization at room temperature[21], as illustrated in Fig. 4e,f. The disruption of the c-Si lattice is generally known to be difficult, because the energy needed to

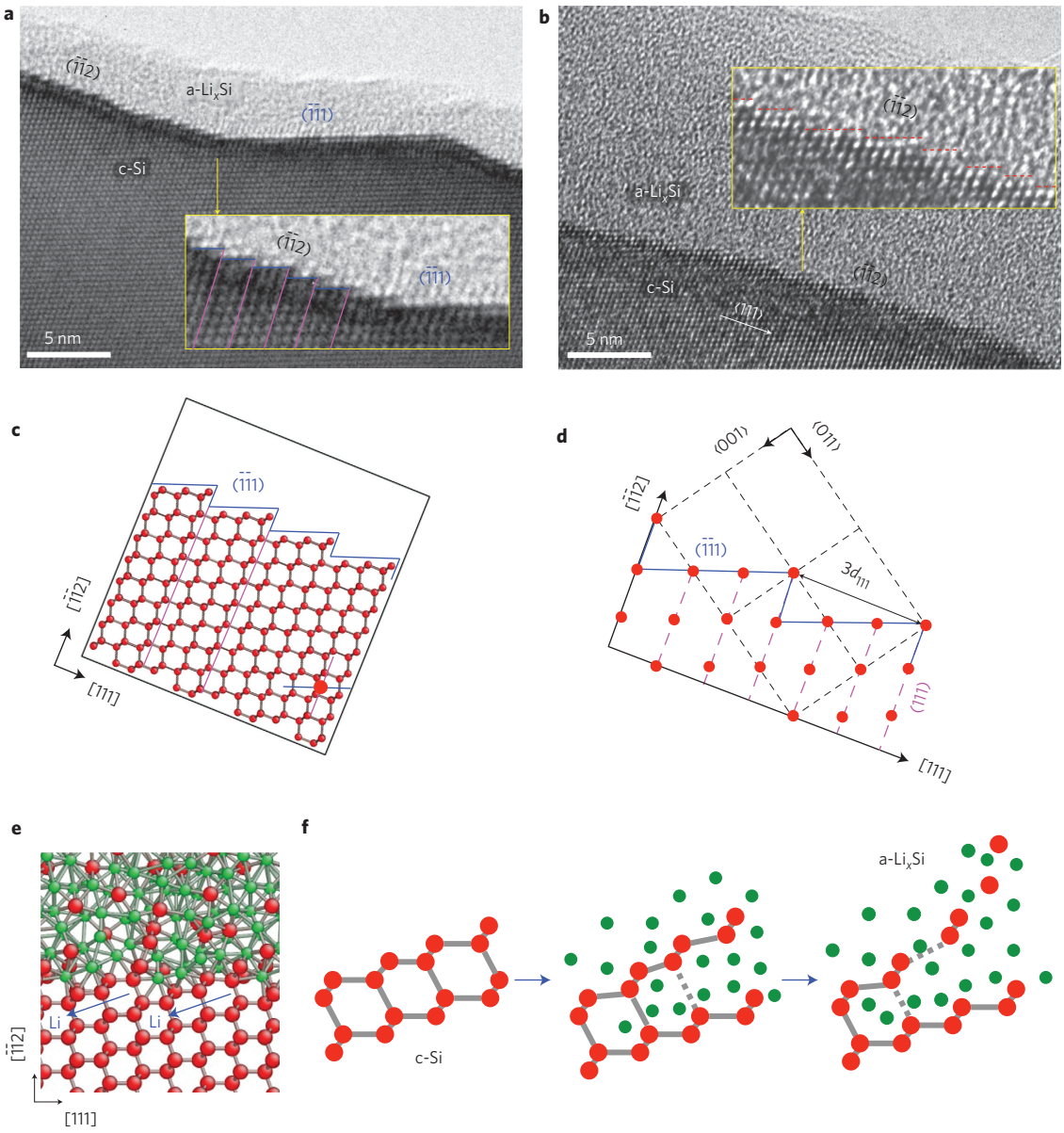

Figure 4 | Atomically resolved structure of the ACI. a, High-resolution TEM image at the early stage of lithiation, showing the {112} ACI with a long smooth {111} facet in the middle and a series of short, inclined {111} atomic facets on the two sides. **b**, The {112} ACI in the late stage of lithiation, with short {111} atomic facets surviving. **c**, Reconstructed atomic structure of a {112} ACI based on the inset image in **a**, showing that an exact {112} ACI actually consists of a series of periodic {111} atomic facets. **d**, Geometrical origin of the periodicity ($3d_{111}$) of {111} atomic facets. Red dots reveal the repeating units in the face-centred cubic lattice; each dot contains two silicon atoms in the adjacent {111} atomic sheets, as indicated by the big red dot in **c**. **e**, Relaxed atomic structure of a {112} ACI from molecular orbital theory calculations (see Methods), showing the high local concentration of lithium atoms (green) that invade the exposed {112} surface of the c-Si (red). **f**, Proposed mechanism of solid-state amorphization based on TEM observations: silicon atoms break away from the c-Si by a mechanism with low energy barriers, in which several lithium atoms enclose a single silicon or a Si–Si pair located near the edge of {111} atomic facets, weaken the Si–Si covalent bonding, and cause the easy dissociation of c-Si.

remove a silicon atom from the low-index smooth surface of c-Si has been measured to be a large fraction of the formation energy of a vacancy in c-Si (2.4–3.5 eV)[22]. This usually causes the rate of silicon dissociation from c-Si to be extremely low at room temperature. However, near the ACI (Fig. 4e), the local lithium concentration is high in the lithium-rich a-Li$_x$Si phase, facilitating an interfacial process of several lithium atoms enclosing a single silicon or Si–Si pair at the edge of {111} atomic facets[23,24]. A previous study of silicide formation indicates that a group of metallic atoms (lithium in this case) can collectively weaken the Si–Si covalent bonding by electron transfer[22]. This leads to the easy dissociation of silicon atoms from c-Si at the ACI (Fig. 4f), thereby resulting in solid-state amorphization with high rates at room temperature. The resulting high mobilities of ACIs are essential for the high-rate capability of batteries. In addition, the applied voltage and doping can further increase the rate of electron/ion transport and interfacial reaction, thus enhancing the amorphization rate[25]. Nevertheless, the lithium-rich local environment near the ledges of {111} atomic facets of an ACI appears to be the key to enabling the fast processes of electrochemically driven solid-state amorphization in c-Si, which become observable in the time window (that is, minutes) of the TEM experiments.

In contrast, the low mobility of an atomically flat {111} ACI can be attributed to the low density of ledges, particularly the high

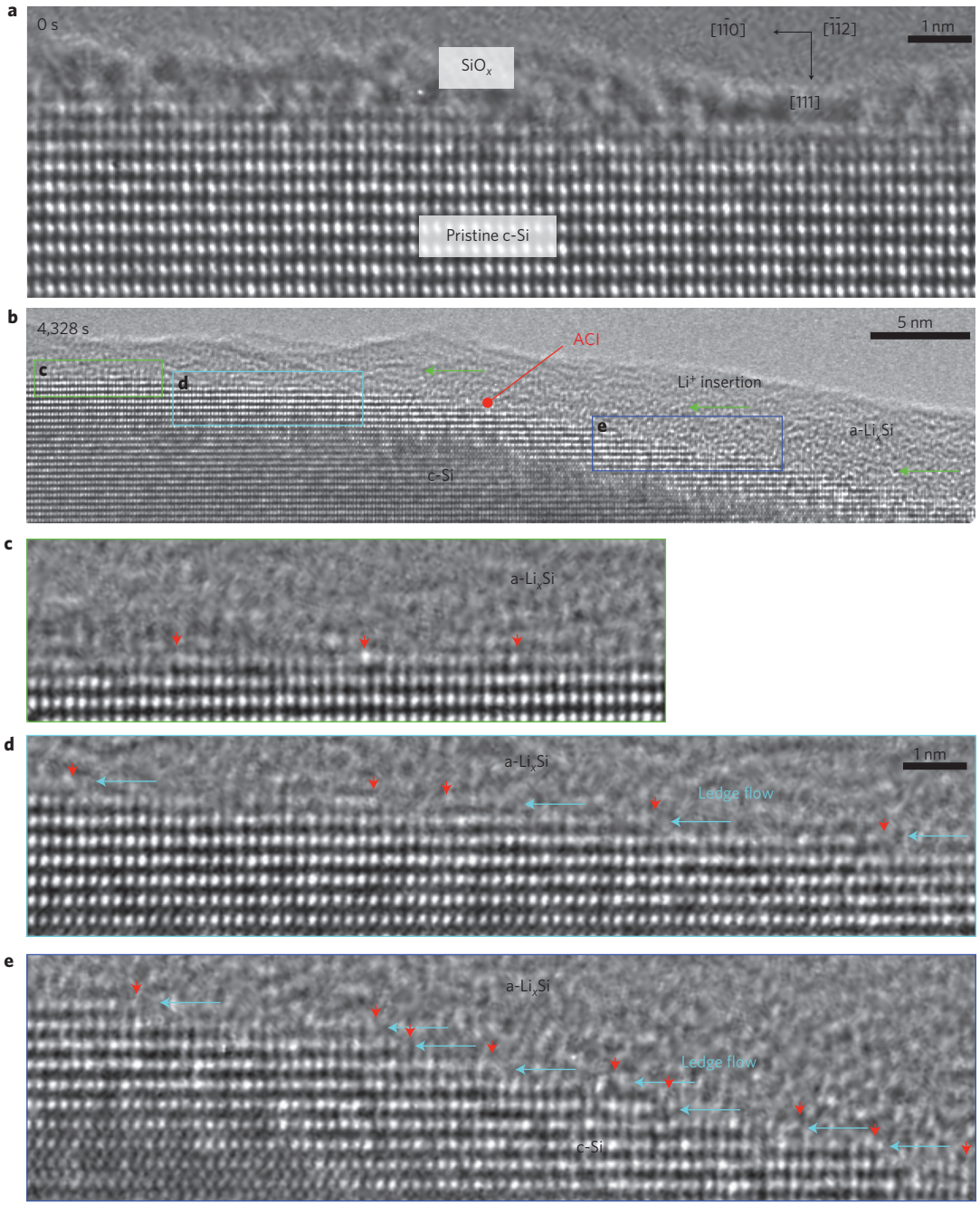

Figure 5 | Ledge mechanism observed in a ⟨110⟩-oriented silicon nanowire during lithiation. a, High-resolution image of the pristine silicon nanowire with a flat (111) surface and 1-nm-thick SiO_x layer. **b**, Morphology of the partially lithiated silicon nanowire. With fast Li^+ transport via surface diffusion, lithiation proceeds along ⟨111⟩ from top to bottom (that is, from surface to core) and via ledge flow along ⟨110⟩ from right to left (marked by green arrows). **c**–**e**, Enlarged zones showing vertical etching of the flat {111} plane, formation of ledges, and ledge-flow-dominated lithiation, respectively. Red arrows indicate ledges and cyan arrows ledge-flow directions. These images represent different stages of lithiation, and the ACI was gradually tilted towards ⟨110⟩.

energetic cost of repeated nucleation of ledge pairs. To reveal how the {111} ACI migrates, Fig. 5 shows the ACI structures in a ⟨110⟩-oriented silicon pillar. Initially, this wire exhibits an atomically flat {111} side surface (Fig. 5a), which is a projected view along the ⟨112⟩ direction. Upon lithiation, lithium atoms quickly transport along the surfaces and insert into the c-Si bulk lattice. Compared with {112} ACIs, the movements of {111} ACIs take a much longer time (the image in Fig. 5b was taken 4,328 s after Fig. 5a). In Fig. 5b, lithium insertion occurs from right to left (marked by green arrows), so the local atomic structures at different sites (enclosed by rectangles denoted c, d and e to link with Fig. 5c–e) represent different stages of lithiation. Intriguingly, the ledge mechanism is seen again, including the formation of ledge pairs on the atomically flat {111} plane (Fig. 5c), the emergence of long {111} terraces (Fig. 5d), and shortening of the terraces by lateral movement of ledges (Fig. 5e). Because a TEM image is a two-dimensional projection and the {111} planes are not infinitely large in a nanowire, it is worth noting that the formation of the ledge pairs in Fig. 5c, defined as two opposite ledges of an outermost {111} layer, might not be produced by lithium penetration through the close-packed plane (that is, ledge flow along the incident electron beam direction could also produce the morphology). As a result

of ledge flow within the {111} layer, the width of the {111} terraces is reduced and the density of ledges on the ACI increased. Meanwhile, the ACI is tilted from the slow-moving directions (⟨111⟩) towards the fast-moving directions (⟨110⟩). The rotation of the {111} ACI towards the fast-moving {110} ACIs in this ⟨110⟩-oriented silicon nanowire is similar to the case of ⟨111⟩-oriented silicon nanowires where the {111} ACIs are reoriented to the fast-moving {112} ACIs (Fig. 4). These results lend further support to the notion that the migration of ACIs occurs through the {111} facet- and ledge-mediated mechanism.

The ledge-mediated mechanism of anisotropic c-Si lithiation provides a mechanistic basis for understanding its morphological evolution and failure. For example, recent experiments have shown a strong orientation dependence of morphological changes in lithiated silicon nanowires and microslabs[13,16,17]. It was observed that the lithiated silicon undergoes a large expansion (~100% linear strain) in the ⟨110⟩ direction, but a considerably smaller expansion (~10% linear strain) in the ⟨111⟩ direction. To understand such anisotropic swelling, we developed a diffusive reaction and elastic–plastic deformation model to simulate the morphological changes during the lithiation of silicon nanowires[13,26]. Our model was based on the key results from the above atomically resolved *in situ* TEM experiments. The ledge-mediated lithiation mechanism leads to a strong orientation dependence of the interfacial mobility; that is, the {110} and {112} ACIs move at least an order of magnitude faster than the {111} ACI. Such highly anisotropic interfacial mobility gives rise to drastically different swellings in different orientations. In other words, to minimize the strain mismatch between the unlithiated and lithiated phases across the ACI, the lithiation strain occurring at the ACI tends to align with the local normal direction of the ACI. This leads to a large expansion along the direction of the fast-moving {110} ACIs and a small expansion in the direction of the slow-moving {111} ACIs. As a consequence of such strongly anisotropic swelling, large, non-uniform tensile plastic flow develops in the lithiated silicon nanowires, which could even result in fracture by self-splitting a single nanowire into two sub-wires[13,27].

Conclusions

We have observed the atomically resolved, dynamic lithiation process in single-crystal silicon nanowires. The *in situ* TEM experiment shows that the lithiation interface between the crystalline silicon and the amorphous product of the Li_xSi alloy is atomically sharp (~1 nm thick). A dynamic ledge mechanism of lithiation-induced solid-state amorphization is revealed, providing a mechanistic understanding of the room-temperature amorphization and orientation-dependent mobilities of the amorphous/crystalline interface. These results provide insights into morphological changes (for example, anisotropic swelling), phase evolution (for example, rate-controlling mechanism) and mechanical degradation (for example, lithiation-induced fracture) during electrochemical alloying of lithium. Our work should motivate research into the interfacial dynamics that govern the rate and deformation behaviour of phase-transforming, high-capacity electrodes, which could be used to build high-performance lithium-ion batteries.

Methods

The ⟨111⟩-oriented silicon nanowires were grown on a heavily doped Si(111) wafer (n-type, electrical resistivity $\rho = 0.001\ \Omega$ cm) via a vapour–liquid–solid mechanism catalysed by 100 nm gold nanoparticles as described elsewhere[28]. $SiCl_4$ precursor diluted in H_2/N_2 was introduced into a horizontal hot-wall chemical vapour deposition reactor and PH_3 (100 ppm in N_2) was used as the dopant source. Epitaxial silicon nanowires with lengths of ~6 μm and diameters of ~130 nm were obtained from a 4 min growth at 900 °C and 600 torr. The as-synthesized silicon nanowires were examined with a field-emission scanning electron microscope (FE-SEM, Hitachi 4700) operated at 21 kV.

The ⟨110⟩-oriented silicon nanowires were fabricated by top-down etching of a heavily doped silicon (110) wafer (p-type with boron dopant, $\rho = 0.085\ \Omega$ cm). Briefly, electron-beam lithography was used to generate a patterned mask (square array with 20 μm pitch in an area of 7 mm × 7 mm). Silicon pillars with lengths of ~10 μm were obtained by a deep reactive ion etch (in CF_4, SF_6 and Ar mixture gas for ~1 h). A thinning process, comprising sequentially thermal oxidation (1,000 °C in dry O_2), SiO_2 etch (in 5% HF aqueous solution) and critical point drying, was repeated over several times to reduce the diameter of the silicon pillars.

To build a nanoscale battery for the *in situ* TEM study, a small piece of silicon wafer with silicon nanowires or pillars was cleaved off from a large silicon wafer substrate and glued to an aluminium rod with conductive epoxy[12,13,19]. This ensured good electrical contact between the nanowires and the silicon substrate, which served as the primary current collector on the silicon nanowire side. Lithium metal was scratched with a tungsten rod inside a glove box filled with helium (O_2 and H_2O content < 1 ppm). Inside the same glove box, both the silicon and lithium electrodes were mounted onto a Nanofactory TEM scanning tunnelling microscope (STM) holder, which was sealed in a home-built air-tight bag filled with dry helium. The holder was quickly transferred into the TEM column and the total time of exposure to air was less than 2 s, which limited the extent of Li_2O formation on the surface of the lithium metal. The thin Li_2O layer served a solid-state electrolyte to allow transport of Li^+ ions but not electrons. The TEM (Tecnai F30, FEI) was operated at 300 kV and the column vacuum level was $\sim 1 \times 10^{-7}$ torr. Inside the TEM, the Li_2O/Li terminal was driven to contact an individual silicon nanowire. Lithiation took place after a bias of –2 V was applied on the silicon nanowire with respect to the lithium metal to drive Li^+ transport through the solid-state Li_2O layer grown on the lithium electrode[13]. During lithiation, the electron beam was blocked except for imaging and video recording. The lithiation velocity was measured by comparing the snapshots at different lithiation stages for a given interval.

To understand the atomic structure near the ACIs, we performed quantum chemical molecular dynamics (MD) simulations at the level of molecular orbital theory by using the AM1 method in the commercial package MOPAC. In simulations, we first generated an amorphous phase of a-$Li_{3.75}Si$ by using a melting–cooling MD approach. The resulting amorphous structure appears to be reasonable, as the associated radial and angular distribution functions were close to those of a-$Li_{3.75}Si$ produced by an entirely different approach (activation relaxation technique; ART)[29]. To build an ACI, we embedded an a-$Li_{3.75}Si$ phase within one half of a MD supercell and a c-Si phase in the other half. The system was then relaxed by MD with the zero pressure and constant temperature ($T = 300$ K). Owing to the timescale limitation of molecular orbital theory-based MD, the migration of ACIs could not be simulated to directly match the TEM experiment. However, the MD-relaxed structure of a {112} ACI (Fig. 4e) clearly revealed a key feature of the local atomic environment near the ACI; namely, a number of lithium atoms near the surface of the lithium-rich phase of a-$Li_{3.75}Si$ tend to enclose the silicon atoms near the ledges of inclined {111} atomic facets on the c-Si surface. Presumably those lithium atoms can collectively weaken the Si–Si covalent bonding by electron transfer[22]. Motivated by our TEM observations and previous NMR studies of atomic structures of lithiated silicon[23,24], in conjunction with those MD results, we propose an atomistic mechanism of solid-state amorphization of c-Si at room temperature, as shown in Fig. 4f.

Received 8 March 2012; accepted 5 September 2012; published online 7 October 2012

References

1. Tarascon, J. M. & Armand, M. Issues and challenges facing rechargeable lithium batteries. *Nature* **414,** 359–367 (2001).
2. Beaulieu, L. Y. *et al.* Colossal reversible volume changes in lithium alloys. *Electrochem. Solid-State Lett.* **4,** A137–A140 (2001).
3. Limthongkul, P., Jang, Y. I., Dudney, N. J. & Chiang, Y. M. Electrochemically-driven solid-state amorphization in lithium-silicon alloys and implications for lithium storage. *Acta Mater.* **51,** 1103–1113 (2003).
4. Kang, B. & Ceder, G. Battery materials for ultrafast charging and discharging. *Nature* **458,** 190–193 (2009).
5. Goodenough, J. B. & Kim, Y. Challenges for rechargeable Li batteries. *Chem. Mater.* **22,** 587–603 (2010).
6. Balke, N. *et al.* Nanoscale mapping of ion diffusion in a lithium-ion battery cathode. *Nature Nanotech.* **5,** 749–754 (2010).
7. Huang, J. Y. *et al. In situ* observation of the electrochemical lithiation of a single SnO_2 nanowire electrode. *Science* **330,** 1515–1520 (2010).
8. Chan, C. K. *et al.* High-performance lithium battery anodes using silicon nanowires. *Nature Nanotech.* **3,** 31–35 (2008).
9. Lee, S. W. *et al.* High-power lithium batteries from functionalized carbon-nanotube electrodes. *Nature Nanotech.* **5,** 531–537 (2010).
10. Zhang, H., Yu, X. & Braun, P. V. Three-dimensional bicontinuous ultrafast-charge and -discharge bulk battery electrodes. *Nature Nanotech.* **6,** 277–281 (2011).
11. Obrovac, M. N. & Christensen, L. Structural changes in silicon anodes during lithium insertion/extraction. *Electrochem. Solid-State Lett.* **7,** A93–A96 (2004).
12. Liu, X. H. & Huang, J. Y. *In situ* TEM electrochemistry of anode materials in lithium ion batteries. *Energy Environ. Sci.* **4,** 3844–3860 (2011).

13. Liu, X. H. *et al.* Anisotropic swelling and fracture of silicon nanowires during lithiation. *Nano Lett.* **11,** 3312–3318 (2011).
14. Chon, M. J. *et al.* Real-time measurement of stress and damage evolution during initial lithiation of crystalline silicon. *Phys. Rev. Lett.* **107,** 045503 (2011).
15. Liu, X. H. *et al.* Size-dependent fracture of silicon nanoparticles during lithiation. *ACS Nano* **6,** 1522–1531 (2012).
16. Lee, S. W., McDowell, M. T., Choi, J. W. & Cui, Y. Anomalous shape changes of silicon nanopillars by electrochemical lithiation. *Nano Lett.* **11,** 3034–3039 (2011).
17. Goldman, J. L., Long, B. R., Gewirth, A. A. & Nuzzo, R. G. Strain anisotropies and self-limiting capacities in single-crystalline 3D silicon microstructures: models for high energy density lithium-ion battery anodes. *Adv. Funct. Mater.* **21,** 2412–2422 (2011).
18. Porter, D. A. & Easterling, K. E. *Phase Transformations in Metals and Alloys* (Chapman and Hall, 1992).
19. Liu, X. H. *et al. In situ* TEM experiments of electrochemical lithiation and delithiation of individual nanostructures. *Adv. Energy Mater.* **2,** 722–741 (2012).
20. Ross, F. M., Tersoff, J. & Reuter, M. C. Sawtooth faceting in silicon nanowires. *Phys. Rev. Lett.* **95,** 146104 (2005).
21. Johnson, W. L. Thermodynamic and kinetic aspects of the crystal to glass transformation in metallic materials. *Prog. Mater. Sci.* **30,** 81–134 (1986).
22. Tu, K. N. Selective growth of metal-rich silicide of near-noble metals. *Appl. Phys. Lett.* **27,** 221–224 (1975).
23. Key, B. *et al.* Real-time NMR investigations of structural changes in silicon electrodes for lithium-ion batteries. *J. Am. Chem. Soc.* **131,** 9239–9249 (2009).
24. Key, B., Morcrette, M., Tarascon, J. M. & Grey, C. P. Pair distribution function analysis and solid state NMR studies of silicon electrodes for lithium ion batteries: understanding the (de)lithiation mechanisms. *J. Am. Chem. Soc.* **133,** 503–512 (2011).
25. Liu, X. H. *et al.* Ultrafast electrochemical lithiation of individual Si nanowire anodes. *Nano Lett.* **11,** 2251–2258 (2011).
26. Yang, H. *et al.* Orientation-dependent interfacial mobility governs the anisotropic swelling in lithiated silicon nanowires. *Nano Lett.* **12,** 1953–1958 (2012).
27. Lee, S. W., McDowell, M. T., Berla, L. A., Nix, W. D. & Cui, Y. Fracture of crystalline silicon nanopillars during electrochemical lithium insertion. *Proc. Natl Acad. Sci. USA* **109,** 4080–4085 (2012).
28. Krylyuk, S., Davydov, A. V. & Levin, I. Tapering control of Si nanowires grown from $SiCl_4$ at reduced pressure. *ACS Nano* **5,** 656–664 (2011).
29. Huang, S. & Zhu, T. Atomistic mechanisms of lithium insertion in amorphous silicon. *J. Power Sources* **196,** 3664–3668 (2011).

Acknowledgements

Portions of this work were supported by a Laboratory Directed Research and Development (LDRD) project at Sandia National Laboratories (SNL) and partly by Nanostructures for Electrical Energy Storage (NEES), an Energy Frontier Research Center (EFRC) funded by the US Department of Energy, Office of Science, Office of Basic Energy Sciences (award no. DESC0001160). The LDRD supported the development and fabrication of platforms. The NEES centre supported the development of TEM techniques. The Sandia-Los Alamos Center for Integrated Nanotechnologies (CINT) supported the TEM capability. Sandia National Laboratories is a multiprogramme laboratory managed and operated by Sandia Corporation, a wholly owned subsidiary of Lockheed Martin Company, for the US Department of Energy's National Nuclear Security Administration (contract DE-AC04-94AL85000). T.Z. acknowledges support from the NSF (grants CMMI-0758554 and 1100205). J.L. acknowledges support from the NSF (DMR-1008104 and DMR-1120901) and AFOSR (FA9550-08-1-0325). S.L.Z. acknowledges support from the NSF (grant CMMI-0900692).

Author contributions

X.H.L. and J.Y.H. conceived and designed the experiments. S.K., J.Y., S.A.D., A.V.D. and S.T.P. synthesized the nanowire samples. X.H.L. and J.W.W. carried out *in situ* TEM experiments. S.H., F.F., X.H., S.Z. and T.Z. performed MD simulations. X.H.L. performed data analysis. X.H.L., T.Z. and J.Y.H. wrote the paper. S.Z. and J.L. revised the manuscript. All authors discussed the results and commented on the manuscript.

Additional information

Supplementary information is available in the online version of the paper. Reprints and permission information is available online at http://www.nature.com/reprints. Correspondence and requests for materials should be addressed to X.H.L., T.Z. and J.Y.H.

Competing financial interests

The authors declare no competing financial interests.